Design and performance of GMR sensors for the detection of magnetic microbeads in biosensors

J. C. Rife[a*], M. M. Miller[a], P. E. Sheehan[a], C. R. Tamanaha[a],

M. Tondra[b], L. J. Whitman[a]

[a]*Naval Research Laboratory, Washington, DC 20375*

[b]*NVE Corp., Eden Prairie, MN 55344*

Abstract

We are developing a biosensor system, the Bead ARray Counter (BARC), based on the capture and detection of micron-sized, paramagnetic beads on a chip containing an array of giant magnetoresistive (GMR) sensors. Here we describe the design and performance of our current chip with 64 sensor zones, compare its performance with the previous chip design, and discuss a simple analytical model of the sensor micromagnetics. With assay-ready Dynal M-280 microbeads (2.8 μm diameter), our threshold for detection is approximately 10 beads per 200 μm-diameter sensor. Single beads made of solid $Ni_{30}Fe_{70}$ can easily be detected, but they must be made biocompatible. The relatively large size of our sensors helps to improve their practical sensitivity compared with other microsensor-based magnetic particle detectors.

Keywords: Biosensors; GMR; Magnetoresistance; Magnetic microbeads; Magnetic sensors

---

[*] Corresponding author. Tel.: 202-767-4654; fax: 202-767- 3321. *E-mail address:* rife@nrl.navy.mil (J. C. Rife).

Report Documentation Page

Form Approved
OMB No. 0704-0188

1. REPORT DATE	2. REPORT TYPE	3. DATES COVERED
19 MAR 2003		**00-00-2003 to 00-00-2003**

4. TITLE AND SUBTITLE	5a. CONTRACT NUMBER
Design and performance of GMR sensors for the detection of magnetic microbeads in biosensors	5b. GRANT NUMBER
	5c. PROGRAM ELEMENT NUMBER
6. AUTHOR(S)	5d. PROJECT NUMBER
	5e. TASK NUMBER
	5f. WORK UNIT NUMBER
7. PERFORMING ORGANIZATION NAME(S) AND ADDRESS(ES) **Naval Research Laboratory,Washington,DC,20375**	8. PERFORMING ORGANIZATION REPORT NUMBER
9. SPONSORING/MONITORING AGENCY NAME(S) AND ADDRESS(ES)	10. SPONSOR/MONITOR'S ACRONYM(S)
	11. SPONSOR/MONITOR'S REPORT NUMBER(S)

12. DISTRIBUTION/AVAILABILITY STATEMENT
Approved for public release; distribution unlimited

13. SUPPLEMENTARY NOTES

14. ABSTRACT

15. SUBJECT TERMS

16. SECURITY CLASSIFICATION OF:			17. LIMITATION OF ABSTRACT	18. NUMBER OF PAGES	19a. NAME OF RESPONSIBLE PERSON
a. REPORT	b. ABSTRACT	c. THIS PAGE			
unclassified	**unclassified**	**unclassified**		**34**	

1. Introduction

Biosensors are under intense development for a wide range of applications, from medical diagnostics to countering bio-terrorism. All systems aim to achieve rapid and sensitive detection with low false positive rates, and in many applications it is desirable that the complete system be contained in a low power, compact package and consume minimal reagents. A common approach to detecting biological molecules is to attach to the target molecule a label or "reporter" moiety that produces an externally observable signal. Traditionally, this is accomplished using biomolecular recognition between the target molecule and a specific receptor (e.g. an antibody) that is tagged with the label. The label may be a radioisotope, enzyme, fluorescent molecule, or charged molecule, for example. Methods to sense the attached labels have been developed based on a variety of transduction mechanisms, including optical, electrical, electrochemical, thermal, and piezoelectrical means, as discussed in numerous reviews [1].

Recently magnetic particles have been developed as labels for biosensing. Magnetic labels have several potential advantages over other labels. The magnetic properties of the beads are very stable over time, in particular because this property is not affected by reagent chemistry or subject to photo-bleaching. From a detection standpoint, there is not usually a significant magnetic background present in a biomolecular sample. Furthermore, magnetic fields are not screened by aqueous reagents or biomaterials. In addition, magnetism may be used to remotely manipulate the magnetic particles. Finally, a number of sensitive magnetic field detection devices have been developed that are suitable for biosensing applications, including giant magnetoresistive (GMR) sensors and spin valves [2, 3], piezo-resistive cantilevers [4], inductive sensors [5], superconducting quantum interference devices (SQUIDs) [6-8], anisotropic magnetoresistive (AMR) rings [9], and miniature Hall crosses [10].

We are developing a biosensor system, the Bead ARray Counter (BARC), based on the capture and detection of micron-sized, paramagnetic beads on a chip containing an array of GMR sensors [2, 11-15]. A basic GMR device consists of a pair of magnetic thin films separated by a non-magnetic conducting layer [16]. When an external magnetic field rotates the magnetizations of the magnetic layers towards alignment, spin-dependent electron scattering is reduced at the interfaces within the device, decreasing its electrical resistance. GMR sensors can be microscopic in size and quite sensitive to the presence of micron and smaller sized magnetic particles in close proximity, especially when the sensor size is similar to that of the particle. The development of GMR devices for biosensing has greatly benefited from the development of advanced magnetic materials and devices for data storage applications, such as hard disk drives and magnetic random access memory (MRAM) [17, 18].

The general approach we use in the BARC biosensor system is illustrated in Fig. 1. As for many other systems, labeling is accomplished using specific ligand-receptor interactions in a "sandwich" configuration. First, receptor molecules specific for the target biomolecules are attached to the surface of the chip above the sensors. Arrays of different probe spots can be used to simultaneously detect multiple targets. The sample solution is flowed over the chip, and target molecules present are captured on to the surface by biomolecular recognition. Magnetic particles coated with a second set of receptor molecules for the target are then introduced, labeling the previously captured targets. We then apply a magnetic field gradient to create a controlled vertical force on each bead that selectively pulls off only those beads not bound to the surface by specific binding. This force discrimination assay increases the sensitivity of detection by greatly reducing the background bead density and thereby permitting very low bead densities to be detected with confidence [12, 19]. Finally, an AC magnetic field is applied, magnetizing the

beads to generate sensing fields. The number of beads over a sensor is then determined by comparing its resistance with that of a protected reference sensor on the chip and two off-chip resistors in a Wheatstone bridge using lock-in detection. The BARC approach has been applied to the detection of DNA, and is currently being adapted for sandwich immunoassays.

In the current prototype BARC system (a tabletop apparatus), the assay is performed inside a flow cell mounted over the sensor chip [12, 14]. The chip itself is wire-bonded to a printed circuit board housed in a disposable plastic cartridge that contains all the required reagents. The cartridge plugs into an automated electronic controller and connects to a miniature pumping system. Fairly complete descriptions of the system have been published previously, including our first array-based GMR sensor chip (BARC-II) with eight sensor zones [2]. In this paper we describe the design and micromagnetic performance of a larger chip with 64 sensor zones (BARC-III), compare its performance with the previous chip design, and discuss a simple analytical model that accounts for the magnetic response of our sensors.

2. Sensor design and instrumentation

2.1. GMR sensor chip design

There have been two generations of multi-zone BARC chips, BARC-II and BARC-III [20]. Both use current-in-plane (CIP) thin-film sensors, which exhibit a decrease in resistance when a magnetic field is directed along a sensing axis in the plane of the GMR film. BARC-II incorporates 66 GMR resistor traces, 5 μm × 80 μm, tied to two ground leads, for a total of 68 pin-outs. The sensor traces are grouped in eight sensing zones each containing a cluster of eight traces, so that each ~250 μm-diameter zone can be functionalized with a receptor probe for a different target. The two remaining sensors on the chip are used as reference sensors in the Wheatstone bridge. Each sensor trace is composed of an uncoupled magnetic/non-

magnetic/magnetic GMR sandwich [21] with a resistance of 220 Ω. In operation, a bias current of about 10 mA is required in order to magnetize the upper layer opposite to the lower one (with the magnetization in-plane and perpendicular to the long axis of the trace). The BARC-II sensors have a relatively low saturation field (~5 mT) and a maximum GMR effect ($\Delta R/R$) of ~5%.

The BARC-II chip has a number of shortcomings that inspired its replacement. Because of the relatively large currents and power dissipation per unit area, the BARC-II sensors generate considerable heat even when biased one-at-time, raising the temperature of the fluid in the flow cell by up to 20 °C during read-out. Although the individual sensor geometry was optimized for the detection of individual, 2.8 μm-diameter, commercial paramagnetic beads, the constraints associated with the required fan-out and the limitations of the biomolecular probe arraying required the sensors to be spaced relatively far apart. Because beads are only detected on or next to a sensor trace, the active area is only ~10% within each sensing zone. The latest chip, BARC-III, was designed to overcome these limitations while simultaneously increasing the number of sensing zones from eight to 64.

Optical micrographs of the BARC-III chip are shown Fig. 2. Like the BARC-II chip, it includes 64 individually addressable GMR sensors and two reference sensors with 68 pin-outs, so it is compatible with the original mechanical scheme for connecting to the control electronics. On BARC-III, however, each sensor is a serpentine resistor trace 1.6 μm wide on a 4.0 μm pitch, with a total length of 8 mm within a 200 μm-diameter circular zone. The zone is well matched to our ~250 μm-diameter arraying system [15], increasing the active area per biomolecular spot by ~10 times over BARC-II. Finally, each sensor has a resistance of 42 kΩ and does not require

a bias current for operation (because of the different GMR design), and therefore dissipates very little power and generates negligible heat.

The BARC-III sensors are composed of a different multilayer GMR material [22] than BARC-II, with a larger saturation field and GMR effect, ~30 mT and ~15%, respectively. The overall structure of each sensor is illustrated to scale in cross-section in Fig. 3. The GMR multilayer stack was deposited in a Perkin Elmer 2400 vacuum deposition system using several mTorr of Ar for a sputter gas. The basic GMR film structure includes four ferromagnetic layers interspersed with three non-ferromagnetic layers. Antiferromagnetic exchange coupling generates the alternating, opposing magnetizations required for the GMR effect. The ferromagnetic layers have three sub-layers, composed of an internal layer of NiFeCo (chosen for its good linearity and low hysteresis with relatively high magnetic polarization), sandwiched between two thin films of CoFe (to maximize the magnetoresistance of the overall structure). The ferromagnetic alloy compositions, in atomic percent, are $Ni_{65}Fe_{15}Co_{20}$, $Co_{95}Fe_5$, and $Cu_{69}Ag_{27}Au_4$. The film thicknesses were chosen to optimize the antiparallel exchange coupling across the CuAgAu layers while maintaining high sensitivity and linearity. Note that the correct thickness of the CuAgAu non-magnetic layer (1.6 nm) is critical to assuring antiferromagnetic coupling and the desired GMR response. Because of shape anisotropy, the magnetization of each GMR trace naturally lies in the plane of the film, so only the planar components of the induced microbead field will cause an appreciable magnetoresistance change.

Both BARC-II and BARC-III chips are covered with a silicon nitride passivation layer about 1 μm thick in order to protect the circuitry from the corrosive and conductive biochemical reagents. However, the presence of this layer is detrimental to sensor performance because of the strong dependence of the GMR signal on the distance of the bead from the sensor (as will be

reviewed below). Because of the anticipated decrease in GMR signal/bead on BARC-III, associated in part with the much larger total area of each trace, the nitride layer was etched down to a final thickness of 250 nm over each sensor zone. The etched regions are evident in the circular rim surrounding each serpentine sensor, seen especially in Figs. 2(b) and 2(c).

2.2. Magnetic bead criteria

The magnetic microbeads used in BARC must have as high a magnetization as possible to maximize the sensor response, and yet remain non-remanent to avoid clustering when suspended in solution. Factors that determine the optimal bead size include the settling times for suspended beads (i.e. their buoyancy), the magnitude of the force that can be applied to the settled beads (to discriminate against biochemical background [12, 19]), and the sensor response. As discussed previously, we have evaluated a number of commercial paramagnetic particles and currently use Dynal M-280 beads [2]. These 2.8 μm-diameter beads are composed of magnetic γ-Fe_2O_3 and Fe_3O_4 nanoparticles (<20 nm in diameter) dispersed in a polymer matrix, with an average magnetic content of 12% by weight [23, 24]. The nanoparticles within these beads are often described as superparamagnetic; that is, they are small enough that the ambient thermal energy is greater than the magnetic alignment energy, so they spontaneously demagnetize at room temperature.

Although Dynal M-280 microbeads are extremely monodispersed in size and have excellent biocompatible surface properties, their magnetic properties are not optimal. Besides having a relatively low saturation magnetization, the magnetic content among beads varies widely (with a standard deviation of 72%), and some beads are non-magnetic [2]. With the goal of achieving larger, more consistent signals from our magnetic labels, we are working to develop soft ferromagnetic beads with 100% magnetic content [13]. Our initial efforts have focused on NiFe

beads produced by an industrial carbonyl process that creates polydispersed, polycrystalline spherical particles ranging from approximately 800 nm to 4 μm in diameter. To be usable for biosensing, they must be size-selected, characterized, and the surfaces must be functionalized with stable, biochemical polymer films (an ongoing effort that will not be discussed here). We have had some success at size-selection using dry filtration methods, narrowing the diameter distribution to 1.0±0.5 μm and thereby enabling more accurate materials characterization [25].

The NiFe microbeads have recently been characterized by a variety of techniques [25], revealing that they are composed of nickel nanoparticles within an iron matrix with an overall stoichiometry of $Ni_{30}Fe_{70}$. Their superior magnetic moment is illustrated in Fig. 4, which compares their magnetization with that of Dynal M-280 microbeads measured with vibrating sample magnetometry (VSM) for field strengths used in BARC (up to 6.8 kA/m = 85.6 Oe). Note that the beads were dispersed in epoxy for these measurements to prevent agglomeration. The NiFe microbeads have a susceptibility of ~3 across the range of BARC field strengths, the maximum obtainable for an uniformly magnetized sphere [13]. Because of this property, smaller solid ferromagnetic beads could effectively be used as biomagnetic labels, which would increase the dynamic range of biosensor assays by allowing more labels/unit area (as long as they are spheres greater than approximately 0.2 μm in diameter, where they can be multi-domain and thus non-remanent). The residual remanence indicated in Fig. 4 can lead to weakly bound clustering in solution. The small remanence may be due to a fraction with slightly non-spherical shapes. Work is ongoing to further characterize the magnetic properties of the NiFe microbeads and chemically functionalize them for use in assays.

2.3. Sensor signal instrumentation

The electronic detection of magnetic microbeads on BARC GMR sensors [2, 13] can be summarized as follows. An external AC magnetic field, H_z^0, is applied normal to the chip (the *z*-direction). As illustrated in Fig. 5, an individual bead, magnetized by the external field and resting on the surface above the GMR resistor trace, generates an AC local dipole field, *B*, with planar components sufficient to cause a magnetoresistance change. The single bead magnetic field components directed positively and negatively along the GMR trace both contribute to a reduction in overall sensor resistance (magnetoresistance curve shown in Fig. 6). The resistance changes of the individual beads are independent and additive up to a saturation point (Fig. 7), as will be discussed. The AC change in resistance, $\Delta R/R$, generates an AC voltage change across a DC-biased Wheatstone bridge. The bridge voltage signal is filtered to remove the DC component, amplified 1000 times or more, and detected by a lock-in amplifier synchronized with the applied AC magnetic field. Note that the external field should not be applied until after the beads have settled on the chip and the force discrimination assay has been completed, otherwise undesirable interactions occur between the magnetized beads. In addition, the DC bias on the bridge cannot be too high (≤4 V in our case) or electrical breakdown can occur through the electrolyte and submicron silicon nitride passivation layer, destroying the device.

In order to characterize the individual GMR sensor response as a function of bead density and position while still under optical inspection, measurements were made on a Zeiss Axiotech microscope with the GMR chips mounted on a carrier board and microscope slide. An AC magnetic field of frequency f = 200 Hz was applied with a single electromagnet (EMR1, Magnet Sales, Culver City, CA) mounted on a separate motion stage just below the microscope stage. The field was measured at the position of the BARC chip to have an amplitude of 9.6 kA/m (121 Oe) or 6.8 kA/m (85.6 Oe) rms. The remaining two resistors of the Wheatstone bridge (at 4 V

DC bias) and a filtered preamplifier were kept close to the chip. Because the magnetoresistance is an even function of the magnetic field (Fig. 6), it must be measured with the lock-in amplifier at the second harmonic frequency (2*f*).

There are a number of sources of background at the second harmonic that need to be compensated for in order to accurately measure the GMR signal under the microscope. The AC magnetic field drives an inductive current in the loops on the chip and interconnects, which creates a strong signal across the bridge at the excitation frequency (1*f*). Distortions in the AC driving signal can then create noise at the harmonics. Unlike the custom magnet used in the full BARC system, the single-pole electromagnet used in this set-up has a fountain-shaped field with significant intensity in the plane of the chip, which also contributes a 1*f* background signal. To compensate for this effect, the lock-in zero at 2*f* was set by adjusting the electromagnet position until the in-plane fields were apparently equal at the selected sensor and the on-chip reference sensor. The zero position is sensitive to adjustments as fine as 25 μm because of the non-uniform field, and is different for each sensor.

Once the background signal was zeroed, we measured the GMR signal from individual sensors as a function of the number of beads by pushing individual beads across a BARC chip with a sharpened tungsten tip mounted on a micromanipulator. To observe the signal with higher densities of beads, a flow cell was mounted on the chip and a suspension of beads flowed across the chip. The number and position of the beads was recorded using a CCD camera mounted on the microscope while the lock-in signal was recorded digitally.

3. Sensor performance and analysis

3.1. Bead Micromagnetics

The overall GMR signal for a sensor, $\Delta R/R$, is determined by sensor geometry and the cumulative local magnetoresistance changes associated with individual microbeads. For the weak fields expected from the microbeads, the local magnetoresistance change depends primarily on the strength of the field oriented along the trace or sensing axis, B_x (see Fig. 5). It is only this component of the planar field that is of interest. For a bead of magnetization M and radius a separated from the GMR trace by an overlayer of thickness t, the field B_x at a distance d along the trace and relative to the center of the bead is given by

$$B_x = \mu_0 \, M \, \frac{a^3 (a+t) d}{\left((a+t)^2 + d^2\right)^{5/2}} . \tag{1}$$

As discussed previously [13], this field has a maximum value

$$B_x^0 = 3.6 \left(\frac{\mu_0}{4\pi} \right) \frac{M}{\left(1 + \frac{t}{a}\right)^3} \tag{2}$$

that occurs a distance $d = (a+t)/2$ along the trace. Note that the B_x field decays within a distance of about a along the trace and $a/2$ across the trace [Fig. 5(b)], with an average magnitude of $B_x^0/\sqrt{2}$ within this $2a \times a$ area. The maximum AC magnetization amplitude, M_{max}, for the excitation field used (9.6 kA/m amplitude) is 3.7 kA/m for a Dynal M-280 and 29 kA/m for a NiFe microbead. For the geometry shown in Figs. 3 and 5 ($t \sim 0.35$ μm), Eq. (2) then yields a maximum magnetic field amplitude at the BARC-III sensor of 0.68 mT for a Dynal M-280 microbead, and 5.9 mT for a NiFe microbead of the same 2.8 μm diameter . For a BARC-II sensor ($t \sim 0.86$ μm), the analogous fields are 0.32 mT and 2.7 mT, respectively.

3.2. Sensor GMR Response

Measurements of the overall magnetoresistance of the BARC-III sensors were made in a large computer-controlled electromagnet oriented along the trace direction with both large and small magnetic-field excursions, as displayed in Fig. 6. For the large field excursions of ±0.11 T, the GMR signal has a substantial butterfly hysteresis around zero. However, for the much smaller field excursions of ±20 mT (closer in magnitude to that from a magnetized Dynal M-280), the hysteresis loops nearly merge, yielding an approximately quadratic magnetoresistance response. In a sinusoidal applied magnetic field at frequency f, the quadratic dependence causes a GMR signal at $2f$ of $C_0 B_x^2$, where $C_0 = 760\ \mathrm{T}^{-2}$. Note that the magnetoresistance change caused by a field normal to the trace (B_y) is also quadratic, but about nine times smaller. The BARC-II sensor magnetization has a quadratic response under all fields (not shown), with an average coefficient $C_0 = 8900\ \mathrm{T}^{-2}$.

The AC change in the GMR sensor resistance, $\Delta R/R$, is detected as an AC voltage change across a DC-biased Wheatstone bridge, $\Delta V \cong V_{dc}\Delta R/4R$ (neglecting a small, second order term). If we approximate the *local* GMR response from one magnetized bead centered on the trace, $\Delta R_l/R_l$, as that caused by a uniform field $B_x^0/\sqrt{2}$ over an area $2a \times a$, the total change in resistance can be approximated as

$$\frac{\Delta R}{R} \approx \left(\frac{2a}{L}\right)\left(\frac{a}{w}\right)\left(\frac{\Delta R_l}{R_l}\right), \tag{3}$$

where L and w are the GMR trace length and width, respectively, and $a<w$. If we further assume the sensor responds locally as it would to a uniform field of equal magnitude (i.e., quadratically as in Fig. 6), then the total resistance change will be

$$\frac{\Delta R}{R} \approx C_0\left(\frac{a^2}{wL}\right)\left(B_x^0\right)^2. \tag{4}$$

Therefore, from Eqs. (2) and (4), the rms AC bridge voltage at $2f$ expected for a single bead centered over a sensor trace can be approximated as

$$\Delta V \approx 1.14 \cdot V_{DC} C_0 \left(\frac{a^2}{wL} \right) \left(\frac{\mu_0}{4\pi} \right)^2 \frac{M_{\max}^2}{\left(1 + \frac{t}{a} \right)^6} \quad . \tag{5}$$

The signals per bead expected from Eq. (5) and those measured for Dynal M-280 microbeads and $Ni_{30}Fe_{70}$ beads of 2.8 μm diameter are listed in Table 1. The calculated results are for an applied field of 9.6 kA/m (6.8 kA/m rms) based on the chip structure of Fig. 3 and the measurements of Figs. 4 and 6 (and comparable measurements for BARC II sensors). The experimental values are for a single bead manipulated onto the center of sensor traces, except in the case of Dynal beads on BARC-III. In that case, the value is based on a series of measurements with beads placed randomly from solution (Fig. 7). In order to approximate the signal per *centered* microbead, the measured signal was multiplied by 1.5. That factor was estimated from measurements of the single bead response of the GMR sensor to bead position across the GMR trace. The actual $Ni_{30}Fe_{70}$ measurements were made with a 3.3 μm-diameter bead. The tabulated results in those cases were scaled to what would be expected for a 2.8 μm diameter using the factor of $a^2/(1+t/a)^6$ from Eq. (5).

The measured single sensor responses per bead agree well with our expectations, demonstrating that a relatively simple micromagnetic analysis can be combined with measured macroscopic magnetic properties to accurately predict sensor performance. Given the signal-to-noise (*S/N*) of the bench-top setup used for these measurements (to be discussed below), a minimum of ~10 Dynal M-280 beads on a BARC-III sensor are required for a detectable signal. However, the apparent *S/N* advantage of the BARC-II sensor is misleading. Although single Dynal beads can be detected, the effective detection area is about 10 times smaller per equivalent

sensing zone, and the BARC-II sensor array has a much smaller intrinsic dynamic range. The >30 times larger signals generated by the solid NiFe microbeads demonstrate their potential superiority as labels for biosensing if they can be prepared with stable, functional surfaces.

As bead density increases, the opposing dipole fields of adjacent beads should reduce the average induced field and the resultant average GMR signal per bead. The measured bridge signal vs. Dynal M-280 coverage is shown in Fig. 7 for beads deposited from solution onto a BARC-III sensor. The ideal, hexagonal close packed limit for 2.8 μm beads within a 200 μm-diameter is about 4630 beads, with the maximum randomly-packed limit expected to be 54.6% of the ideal [26], or about 2530 (a number we nearly achieved). We find the sensor signal is linear with bead density to about 1000 beads, giving us three decades of dynamic range per sensor, with an AC bridge output of 15 nV rms per randomly-placed Dynal M-280 bead. We attribute the departure from linearity above ~1000 beads—where the average bead separation approaches a bead diameter—to the expected decrease in local magnetic field per bead caused by their opposing dipoles. A simple calculation for 2.8 μm beads in a hexagonal array shows that the external field is effectively reduced by 9% for beads separated by a 2.8 μm gap (1156 beads), and 23% when the gap is reduced to 1 μm (2530 beads).

As discussed above, a magnetized microbead creates a fairly local field in the plane of the sensor trace. We examined the dependence of the GMR response on bead position across a wide area of the serpentine BARC-III sensor using Magnetoresistance Sensitivity Mapping (MSM) [9, 27]. For these measurements, we attached a 4.35 μm-diameter NiFe bead to an atomic force microscope (AFM) cantilever using epoxy. The bead was then used as the imaging tip to record the topography of the sensor chip, shown in Fig. 8(a), albeit with low spatial resolution and significant feature distortion from the large tip radius. While the topography was recorded, the

GMR bridge signal was simultaneously recorded via the same electronics and magnetics instrumentation used for the other sensor response measurements. The resulting MSM "image" is shown in Fig. 8(b). The MSM image reveals interesting variations in the local GMR response both along and across the traces. Along the traces, the GMR signal varies by about ±30%. We attribute these variations either to non-perfect GMR trace edges leading to differences in magnetization edge-pinning (and possibly magnetic shorting), or to a non-perfect GMR multilayer stack, particularly considering the critical 1.6 nm thickness of the non-magnetic CuAgAu coupling layer. However, film thickness variations on this scale are not resolvable in the AFM topographs.

3.3. Signal-to-noise analysis

The bridge signal from a single BARC-III sensor is limited to voltages between 10^{-7} and 10^{-8} of the bridge bias by Johnson noise, *1/F* noise, and drift of the GMR zero. The Johnson noise for the sensor resistance of 42 kΩ is 26 nV/√Hz rms. Spectral analysis of the signal with a sensor covered with Dynal M-280 beads showed a *1/F* background of 300 nV/√Hz at the 400 Hz second-harmonic measurement frequency. A large *1/F* background for GMR multilayers has been directly associated with the GMR effect and GMR anti-ferromagnetic order at the low fields in which our sensor operates [28], and there may be an additional contribution from Barkhausen noise caused by the AC magnetic field [29]. Note that at higher frequencies the *1/F* noise drops to a Johnson noise floor (with a corner frequency of about 1.5 kHz). An additional source of noise in actual measurements is the FET preamp, at 6 nV/√Hz.

During actual measurements of the sensor response with Dynal beads, the noise level of the bridge output was typically about 40 nV rms (25 s average). Measurements over 30 min showed

slowly-varying, base-line drifts of up to 200 nV. This drift can cause errors when performing biosensing assays under the microscope because of the 15–20 min that elapse between zeroing the GMR signal and completing the assay. We suspect the greatest contributor to this drift may be small changes in the mechanical position of the magnet with respect to the microscope stage, which has a strong effect on the zero setting. Although the active sensors are in principle thermally compensated by the proximity of the reference sensor in the Wheatstone bridge, the relatively large temperature dependence of the GMR resistance (+0.14%/°C) may also contribute if slowly varying temperature gradients exist. These sources of drift should be reduced when the assays are performed within the BARC instrument enclosure, where the magnetic field is more uniform and the mechanical mounting is more robust.

For a BARC-III sensor, the *S/N* of the rms bridge voltage for a single, randomly placed Dynal M-280 bead is about 1/3 over the short term, but only 1/13 with the long term drift. Therefore, our average GMR detection limit is ~10 M-280 beads or a single, similar-size NiFe bead. Although the base-line drift can be improved mechanically, the remaining *S/N* depends on both the instrumentation and the micromagnetics. Taking the noise as purely *1/F*, the *S/N* will scale as

$$\frac{S}{N} \propto \frac{M^2}{\left(1+\frac{t}{a}\right)^6} \frac{a^2\, F^{1/2}\, h^{1/2}}{w^{1/2}\, L^{1/2}\, \gamma^{1/2}} \quad . \tag{6}$$

This equation assumes the *1/F* noise follows the rule-of-thumb Hooge formula [30], where the voltage fluctuation power spectral density is given by $\gamma V^2/NF$ where γ is the Hooge constant and N is the number of charge carriers in the GMR sensor (for metals $N \sim$ the atomic number density * L * w * h where h is the thickness of the GMR film). If the measurement frequency is increased to 1.5 kHz, the noise can be reduced to the Johnson noise floor, proportional to the

square root of the sensor trace resistance. Then the *S/N* for a single bead will depend only on the magnetization and geometrical factors as

$$\frac{S}{N} \propto V_{DC} \frac{M^2}{\left(1+\frac{t}{a}\right)^6} \frac{a^2}{w^{1/2} L^{3/2}} . \quad (7)$$

In addition to reducing the noise, we can increase the signal in a number of ways. The signal increases with bead magnetization as M^2, which can be accomplished with higher magnetization beads and/or with higher magnetizing fields. At the field magnitudes we presently use, the higher magnetization NiFe beads can provide a signal improvement >30 times over the Dynal M-280 beads of the same size. Moreover, because of the higher saturation fields of NiFe beads, they offer the potential for even further signal enhancement by using higher excitation fields (Fig. 4). Signal levels can also, in principle, be increased with diminishing returns by further decreasing the silicon nitride layer thickness. Calculations using Eq. (5) predict a signal increase of about 1.9× if the current thickness is halved to 0.18 μm, and about 2.6× if it is halved again to 0.09 μm. However, our past experience indicates thinner films would lead to shorting problems in the saline solutions used. Finally, as demonstrated by the performance of BARC-II sensors, greater signal/sensor can be achieved with shorter traces. However, to maintain the overall sensing area, such a change would entail a much larger number of sensing elements, requiring the on-chip integration of multiplexing electronics in order to maintain a reasonable number of pin-outs.

4. Comparison with other magnetic labeling and sensing approaches

Magnetic labeling and detection of biomolecules has been demonstrated with a variety of magnetic particles, from magnetite nanoparticles to polymer matrix microbeads, detected with a

range of approaches, from liquid nitrogen-cooled SQUIDs to Hall cross semiconductor-based electronic devices. Because of the different magnetic properties and sizes of the various particles used, it is difficult to directly compare the sensitivities of the different approaches without considering some practical aspects of biosensing.

The actual sensitivity of a biosensor system based on magnetic bead labeling is determined by the assay sensitivity combined with the detector sensitivity. The assay determines how well target biomolecules are captured from the sample into the detection zone and labeled with a magnetic particle. It is only at that point that the detector sensitivity becomes important, determining the minimum number of labels that can be detected. For assays where the targets are passively delivered to the capture surface by diffusion or flow (most cases), it is important to distinguish the *density of labels* within the detection area from the *number of labels,* because the smaller the detection area, the less sensitive the biochemical assay. If we assume that at the dilute limit each particle will label one biomolecule (although a few particles may be attached if they are nanoscale), and that the larger the detection area the more target molecules will be captured per unit time, then one sensitivity figure-of-merit is the sensing area required per detectable magnetic particle.

The published magnetic particle detection limits for a variety of systems are summarized in Table 2. Although other approaches may generate larger *S/N* for smaller particles, BARC-III sensors combined with NiFe microbeads have the largest potential sensitivity assuming passive delivery of target molecules to the sensor. Small, highly-sensitive microsensors will ultimately have the advantage if high density arrays can be integrated and multiplexed on a chip. Moreover, the overall sensitivity of any of these schemes would be enhanced if target

biomolecules can be *actively* directed to the sensing zones; for example, by magnetic, fluidic, or electrochemical forces.

5. Conclusions

We are developing a biosensor system based on the capture and detection of micron-sized, paramagnetic beads on a chip containing an array of GMR sensors. Here we have described the design and micromagnetic performance of our BARC-III chip with 64 sensor zones, compared its performance with our previous chip, and discussed a simple analytical model that accounts well for the magnetic response of our GMR sensor system. With commercial Dynal M-280 microbeads, which have excellent biocompatible surface properties, our threshold for detection is approximately 10 beads per 200 μm-diameter sensor. With solid, soft ferromagnetic NiFe microbeads, single beads can easily be detected. Efforts are underway in our laboratory to functionalize these particles with stable, biochemical polymer films. The relatively large size of our sensors helps to improve their practical sensitivity compared with other microsensor-based detection schemes.

Although we have focused on the detector sensitivity, the actual sensitivity of any biosensor system also depends on the assay performance. The assay performance is determined not only by how well the target biomolecules are captured and labeled in the detection zone, but also by how specific this process is; i.e. the background label density in the absence of target. Even with force discrimination under ideal laboratory conditions, DNA hybridization assays on an arrayed BARC-III chip typically exhibit a background signal of ~10 beads per sensor. Therefore, increasing the GMR signal per bead will increase our *S/N* but not our overall sensitivity. It is important to consider these practical sensing issues when designing, characterizing, and comparing biosensor systems.

Acknowledgements

We are grateful to M. Piani and M. Stevens for their technical assistance. This work was supported by the Office of Naval Research and the Defense Advanced Research Projects Agency.

Table 1

Wheatstone bridge signal per 2.8 μm-diameter microbead

	Dynal M-280		$Ni_{30}Fe_{70}$	
	Predicted	Measured	Predicted	Measured
BARC-II	1.5 μV	2.2 μV	94 μV	105 μV
BARC-III	19 nV	22 nV	1.2 μV	0.72 μV

Table 2

Detection of magnetic particles for biosensing

Detector Type	Detection Area (μm^2)[a]	Particle	Particle Diam.[b]	Sensitivity (particles)	Area per detectable particle (μm^2)
BARC-III	3.1×10^4	$Ni_{30}Fe_{70}$ Dynal M-280	3.3 μm 2.8 μm	1 10	3.1×10^4 3.1×10^3
Microcantilever [4]	2×10^4	NdFeBLa	2 μm	1	2×10^4
BARC-II [2]	3.2×10^3	Dynal M-280	2.8 μm	1	3.2×10^3
Resonant Coil [5]	2.5×10^7	Dynal M-280	2.8 μm	10^5	2.5×10^2
SQUID [6]	1.7×10^5	Magnetite	35 nm	4×10^3	42
Spin Valve [3]	12	Micromer®-M	2 μm	1	12
AMR Ring [9]	8.0	$Ni_{30}Fe_{70}$	4.3μm	1	8.0
Hall Sensor [10]	5.8	Dynal M-280	2.8 μm	1	5.8
SQUID [8]	3.1×10^6	Magnetite	50 nm	1.8×10^6	1.7
SQUID [7]	6.8×10^4	Magnetite	11 nm	10^8	6.8×10^{-4}

[a]The surface area over which particles were captured and detected.

[b]Including polymer coating, when reported.

Biographies

J. C. Rife is a physicist working on biosensors at the US Naval Research Laboratory (NRL). He received a PhD in Physics from the University of Wisconsin in 1976. After a three-year postdoctoral appointment at the National Institute of Standards and Technology (NIST), he joined the NRL staff where he worked on the optical properties of solids using synchrotron radiation, and the development of new kinds of ultraviolet instrumentation. His current research focuses on the development of magnetic bead-based biosensors, including both optical and micromagnetic detection systems.

M. M. Miller is a physicist working on magnetic sensor development at NRL. He received a PhD in Physics from Purdue University in 1987. After a postdoctoral term at Purdue working with high temperature superconductivity, he joined NRL as a National Research Council (NRC) Postdoctoral Fellow in 1989, becoming a staff member in 1992. Since 1994 he has been involved in the study of magnetic multilayers and the development of GMR-based sensors, including the BARC biosensor.

P. E. Sheehan is a chemical physicist working on nanoscale patterning at NRL. He earned a PhD in Chemical Physics from Harvard University in 1997 for work on the nanomechanics of fullerenes and transition metal chalcogenides. After a three year NRC postdoctoral fellow at NRL, he joined the staff in 2001. His current interests include nanometer scale deposition, diffusion processes, biomineralization, and sensor design.

C. R. Tamanaha is a biomedical engineer working on fluidic systems at NRL. He received a PhD in Biomedical Engineering from Worcester Polytechnic Institute in 1997. He has been at NRL since 1997, first as an American Society of Engineering Education Postdoctoral Fellow and

then as a staff member. He is responsible for the design and fabrication of a range of innovative fluidic and microfluidic systems for use with a number of different biosensor devices.

M. Tondra is a research program manager at NVE Corp. working with NRL on the development of the BARC sensor chip. He received a PhD from the University of Minnesota in 1996. At NVE, he is currently working on projects for the development of spin-dependent tunneling memory and magnetic field sensors, magnetic bead-based biological assays, magnetometers, and related electronics systems. His technical expertise includes magnetism, magnetoresistive thin film development, and fabrication process development.

L. J. Whitman is head of the Surface Nanoscience and Sensor Technology Section at NRL, an interdisciplinary team studying the nanometer-scale properties of surfaces, interfaces, and thin films in a wide range of environments, and applying their expertise to the development of electronic devices and sensors. He received a PhD in Physics from Cornell University in 1988, and joined the research staff at the NRL in 1991 after a NRC Postdoctoral Fellowship at NIST. His current research interests include individual semiconductor, organic, and biomolecular nanostructures, their use in novel functional surfaces, and their application to revolutionary biosensor and electronic device technologies.

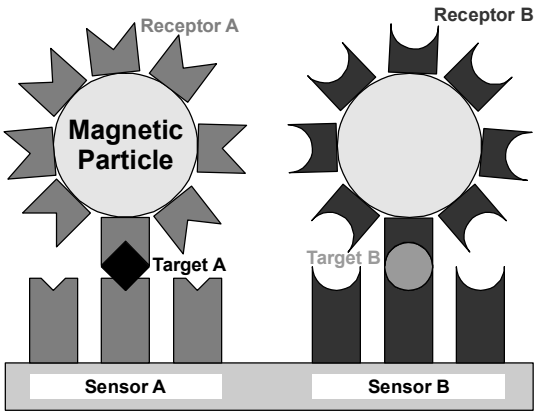

Fig. 1. Generic illustration of magnetic labeling and detection of targets captured onto a solid substrate using specific biomolecular ligand-receptor recognition in a “sandwich” configuration.

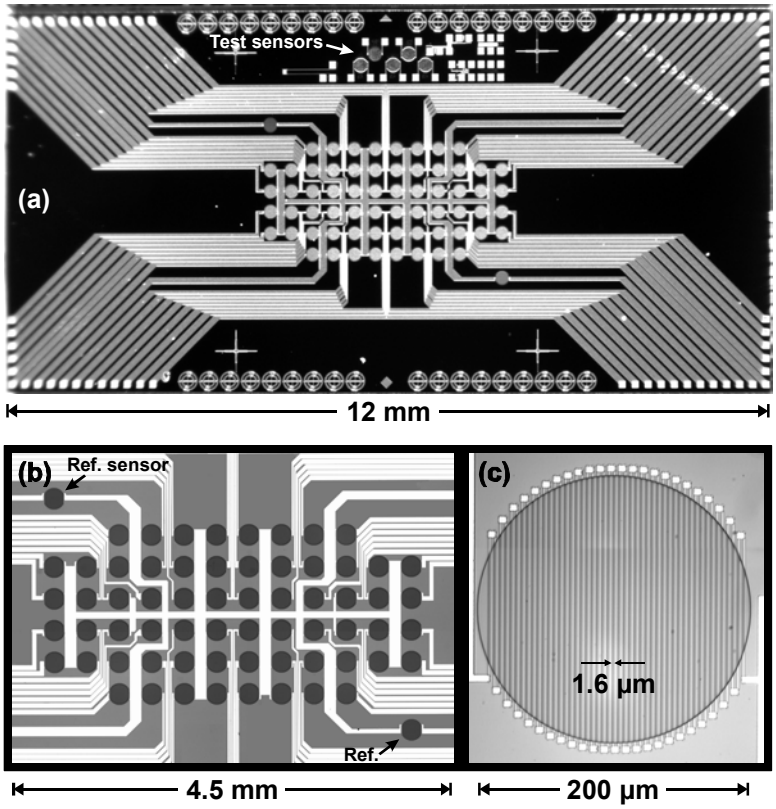

Fig. 2. Optical micrographs of a BARC-III sensor chip. (a) The 68 pin-out chip, including a central sensing area with 64 sensors and two reference sensors, and a number of test structures. (b) Closer view of the central sensing area. (c) Close-up of one serpentine GMR sensor trace encompassing a 200 µm-diameter sensing zone.

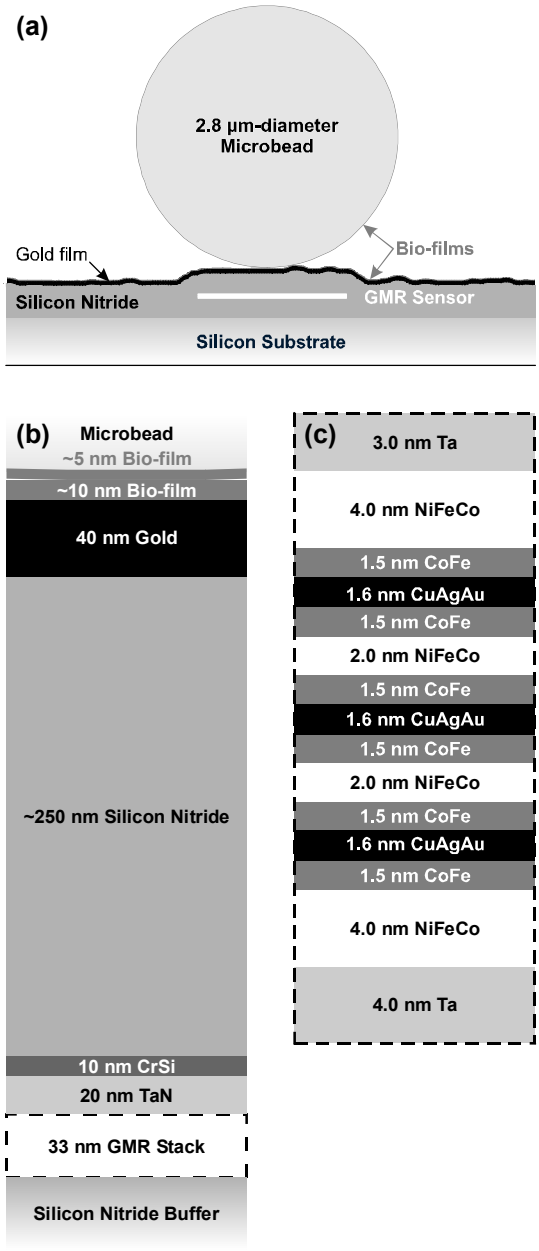

Fig. 3. Cross-sectional, scale illustration of (a) the bead/sensor chip geometry; (b) the multilayer chip design; and (c) the films comprising the GMR stack.

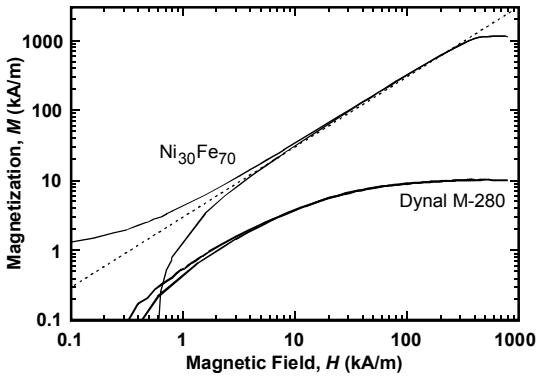

Fig. 4. Volume magnetization as a function of magnetic field for Dynal M-280 and $Ni_{30}Fe_{70}$ microbeads (solid lines) in a vibrating sample magnetometer. The dashed line shows the magnetization of an ideal paramagnetic sphere, $M=3H$ (the theoretical maximum).

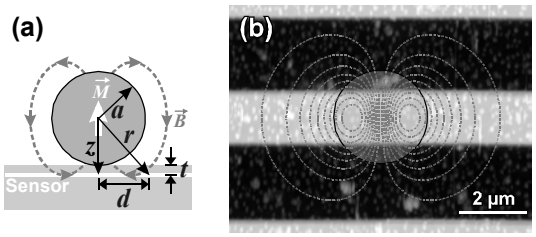

Fig. 5. Illustration of the micromagnetics of a paramagnetic bead under an applied field (in the direction of ***M***). (a) A cross-section of a bead of radius a on top of a sensor separated by an overlayer of thickness t. The dashed lines and arrows indicate the induced magnetic field. (b) An AFM image of a BARC-III sensor trace with the silhouette of a 2.8 μm-diameter bead centered over the trace. The dashed lines are contours of constant induced field in the plane of the sensor for fields oriented along the trace (B_x). Each contour represents a change in intensity of 10% from the B_x^0 maximum, with the outer contour representing 10% of the maximum.

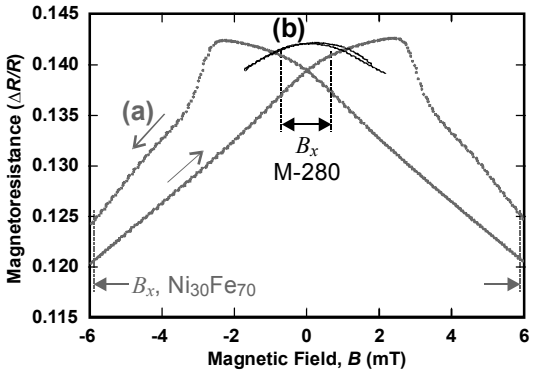

Fig. 6. Magnetoresistance loops measured for a BARC-III sensor with both (a) large (±0.11 T), and (b) small (±20 mT) magnetic-field excursions. The direction of the field change is indicated for the large excursion curve. Note that by convention the magnetoresistance change is referenced to the resistance measured under a saturating field. For reference, field strengths are demarcated corresponding to the local field expected from a magnetized, 2.8 μm-diameter $Ni_{30}Fe_{70}$ or Dynal M-280 microbead.

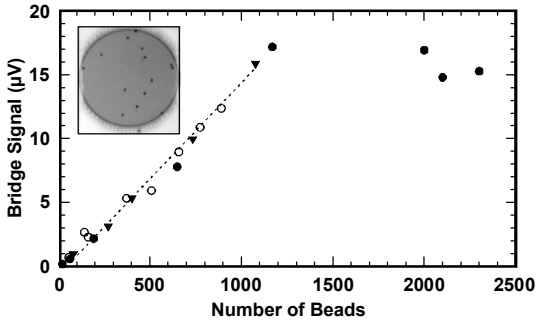

Fig. 7. The Wheatstone bridge signal versus Dynal M-280 coverage for beads deposited from solution onto a BARC-III sensor. The data indicated with open circles, filled circles, and filled triangles were measurement on three separate chips. The dashed line shows a linear fit to the triangles corresponding to 15 nV per bead. Note that some of the filled circle data set has been scaled by a constant factor to adjust for a zeroing error during that measurement. INSET: Optical micrograph of 14 beads on a sensor.

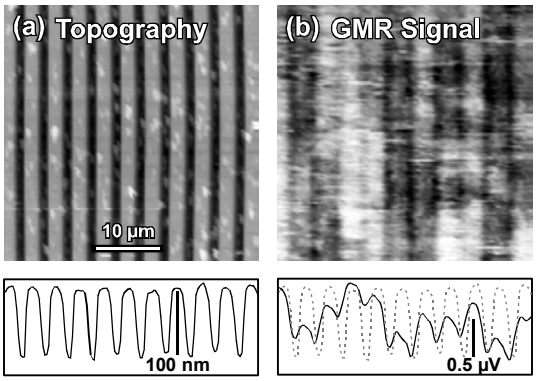

Fig. 8. Magnetoresistance Sensitivity Mapping (MSM) of a BARC-III sensor performed by affixing a 4.35 µm-diameter NiFe bead to an AFM cantilever. (a) The topography of the sensor chip recorded using the bead as the imaging tip, and the average profile across the image. Note there is a significant enhancement of the apparent trace width because of the large tip radius. (b) The GMR bridge signal recorded simultaneously with the topography. In addition to the average profile of the GMR signal, the corresponding topography profile is shown for spatial reference (dashed line). Note that a GMR signal is generated at all bead positions, with the minimum of the trace at 1.28 µV.

References

[1] D. Ivnitski, I. Abdel-Hamid, P. Atanasov, E. Wilkins, Biosensors for detection of pathogenic bacteria, Biosens. Bioelectron. 14 (1999) 599-624.

[2] D.R. Baselt, G.U. Lee, M. Natesan, S.W. Metzger, P.E. Sheehan, R.J. Colton, A biosensor based on magnetoresistance technology, Biosens. Bioelectron. 13 (1998) 731-739.

[3] D.L. Graham, H. Ferreira, J. Bernardo, P.P. Freitas, J.M.S. Cabral, Single magnetic microsphere placement and detection on-chip using current line designs with integrated spin valve sensors: biotechnological applications, J. Appl. Phys. 91 (2002) 7786-7788.

[4] D.R. Baselt, G.U. Lee, K.M. Hansen, L.A. Chrisey, R.J. Colton, A high-sensitivity micromachined biosensor, Proc. IEEE 85 (1997) 672-680.

[5] J. Richardson, A. Hill, R. Luxton, P. Hawkins, A novel measuring system for the determination of paramagnetic particle labels for use in magneto-immunoassays, Biosens. Bioelectron. 16 (2001) 1127-1132.

[6] S. Lee, W.R. Myers, H.L. Grossman, H.M. Cho, Y.R. Chemla, J. Clarke, Magnetic gradiometer based on a high-transition temperature superconducting quantum interference device for improved sensitivity of a biosensor, Appl. Phys. Lett. 81 (2002) 3094-3096.

[7] S. Katsura, T. Yasuda, K. Hirano, A. Mizuno, S. Tanaka, Development of a new detection method for DNA molecules, Supercond. Sci. Tech. 14 (2001) 1131-1134.

[8] K. Enpuku, T. Minotani, T. Gima, Y. Kuroki, Y. Itoh, M. Yamashita, Y. Katakura, S. Kuhara, Detection of magnetic nanoparticles with superconducting quantum interference device (SQUID) magnetometer and application to immunoassays, Jpn. J. Appl. Phys. 2 38 (1999) L1102-L1105.

[9] M.M. Miller, G.A. Prinz, S.F. Cheng, S. Bounnak, Detection of a micron-sized magnetic sphere using a ring-shaped anisotropic magnetoresistance-based sensor: a model for a magnetoresistance-based biosensor, Appl. Phys. Lett. 81 (2002) 2211-2213.

[10] P.A. Besse, G. Boero, M. Demierre, V. Pott, R. Popovic, Detection of a single magnetic microbead using a miniaturized silicon Hall sensor, Appl. Phys. Lett. 80 (2002) 4199-4201.

[11] D.R. Baselt, Biosensor Using Magnetically Detectable Label, U.S. Patent 5,981,297, Nov. 9, 1999.

[12] R.L. Edelstein, C.R. Tamanaha, P.E. Sheehan, M.M. Miller, D.R. Baselt, L.J. Whitman, R.J. Colton, The BARC biosensor applied to the detection of biological warfare agents, Biosens. Bioelectron. 14 (2000) 805-813.

[13] M.M. Miller, P.E. Sheehan, R.L. Edelstein, C.R. Tamanaha, L. Zhong, S. Bounnak, L.J. Whitman, R.J. Colton, A DNA array sensor utilizing magnetic microbeads and magnetoelectronic detection, J. Magn. Magn. Mater. 225 (2001) 138-144.

[14] C.R. Tamanaha, L.J. Whitman, R.J. Colton, Hybrid macro-micro fluidics system for a chip-based biosensor, J. Micromech. Microeng. 12 (2002) N7-N17.

[15] P.E. Sheehan, R.L. Edelstein, C.R. Tamanaha, and L.J. Whitman, A simple pin-spotting method for arraying biomolecules on solid substrates, Biosens. Bioelectron., in press.

[16] U. Hardman (ed.), *Magnetic Thin Film and Multilayer Systems: Physics, Analysis, and Industrial Applications*, Springer Series in Materials Science, 1996.

[17] G.A. Prinz, Device physics - magnetoelectronics, Science 282 (1998) 1660-1663.

[18] J.G. Zhu, Y.F. Zheng, G.A. Prinz, Ultrahigh density vertical magnetoresistive random access memory, J. Appl. Phys. 87 (2000) 6668-6673.

[19] G.U. Lee, S. Metzger, M. Natesan, C. Yanavich, Y.F. Dufrêne, Implementation of force differentiation in the immunoassay, Anal. Biochem. 287 (2000) 261-271.

[20] Fabricated by Nonvolatile Electronics, Eden Prairie, MN.

[21] J.M. Daughton, Weakly Coupled GMR Sandwiches, IEEE T. Magn. 30 (1994) 364-368.

[22] J.B. J. Daughton, R. Beech, A. Pohm, and W. Kude, Magnetic field sensors using GMR multilayer, IEEE T. Magn. 30 (1994) 4608-4610.

[23] Dynal, Dynal Biotech, Oslo, Norway.,

[24] W.S. Prestvik, A. Berge, P.C. Mork, P.M. Stenstad, J. Ugelstad, Preparation and application of monosized magnetic particles in selective cell separation, in *Scientific and Clinical Applications of Magnetic Carriers*, Plenum, New York, 1997, pp.11-35.

[25] S. Calvin, M.M. Miller, R. Goswami, S.F. Cheng, S.P. Mulvaney, L.J. Whitman, V.G. Harris, Determination of crystallite size in a magnetic nanocomposite using extended x-ray absorption fine structure, J. Appl. Phys. 94 (2003) 778-783.

[26] P. Schaaf, J. Talbot, Kinetics of random sequential adsorption, Phys. Rev. Lett. 62 (1989) 175-178.

[27] M. Nakamura, M. Kimura, K. Sueoka, K. Mukasa, Scanning magnetoresistance microscopy with a magnetoresistive sensor cantilever, Appl. Phys. Lett. 80 (2002) 2713-2715.

[28] H.T. Hardner, M.B. Weissman, M.B. Salamon, S.S.P. Parkin, Fluctuation-dissipation relation for giant magnetoresistive 1/f noise, Phys. Rev. B 48 (1993) 16156-16159.

[29] H.T. Hardner, S.S.P. Parkin, M.B. Weissman, M.B. Salamon, E. Kita, 1/f noise in giant magnetoresistive materials, J. Appl. Phys. 75 (1994) 6531-6533.

[30] M.B. Weissman, 1/F noise and other slow, nonexponential kinetics in condensed matter, Rev. Mod. Phys. 60 (1988) 537-571.